SRR-Based RF Sensor for Non-Invasive Detection of Static Bone Fracture States

Annals of Emerging Technologies in Computing (AETiC)
Vol. 9, No. 5, 2025

Research Article

SRR-Based RF Sensor for Non-Invasive Detection of Static Bone Fracture States

Prince O. Siaw[1], Ebenezer Adjei[1], Ahmad Aldelemy[1], Aslan N. Moqadam[2], Mohammed Lashab[3] and Raed A. Abd-Alhameed[1,4]

[1]University of Bradford, United Kingdom
p.o.siaw@bradford.ac.uk; e.adjei@bradford.ac.uk; a.a.aldelemy@bradford.ac.uk; r.a.a.abd@bradford.ac.uk
[2]University of Tabriz, Iran
Aslannourimoqadam91@gmail.com; a.nourimoqadam@tabrizu.ac.ir
[3]Oum El Bouaghi University, Algeria
lashabmoh@gmail.com
[4]Al-Farqadein University College, Iraq
r.a.a.abd@bradford.ac.uk
*Correspondence: r.a.a.abd@bradford.ac.uk

Received: 5 June 2025; Accepted: 2 August 2025; Published: 25 October 2025

Abstract: This study presents the design and simulation of a metamaterial-based radio frequency (RF) sensor employing Split-Ring Resonator (SRR) structures for the non-invasive detection of static bone fracture states. Traditional imaging modalities such as X-ray, CT, and MRI, though widely used, often face limitations in accessibility, cost, radiation exposure, and sensitivity to micro-fractures. To address these gaps, the proposed sensor operates within the 1–3 GHz frequency range and leverages dual SRRs to enhance field confinement and sensitivity to dielectric changes caused by bone discontinuities. Full-wave simulations were conducted using CST Microwave Studio on a multilayer femur phantom comprising realistic anatomical layers, including skin, fat, muscle, cortical bone, and blood. The sensor demonstrated a strong response to variations in dielectric properties associated with fracture conditions, achieving detection of fracture features as small as 0.10 mm in width and 20 mm in depth beneath a 5.00 mm thick cortical layer. Reflection coefficient analysis (|S11|) revealed distinct resonance shifts between healthy, fractured, and healed bone states, with frequency deviations up to 47 MHz and quality factors exceeding 80. An iterative antenna design process led to an optimised SRR configuration (ANT 5), exhibiting high Q-factor, enhanced electromagnetic confinement, and excellent impedance matching. The findings highlight the sensor's potential as a compact, non-ionising, and wearable diagnostic tool for orthopaedic applications.

Keywords: ***Biological tissues; Dielectric material; Fracture detection; Metamaterial; Microwave sensor; Split-ring resonator***

1. Introduction

Bone fractures are a pervasive medical condition with significant impacts on both individual health and public healthcare systems. Accurate and early diagnosis is crucial for timely intervention, ensuring proper healing and functional recovery. Delayed or missed diagnoses can lead to severe complications, including non-union, malunion, chronic pain, and impaired mobility. Alarmingly, missed fractures may account for up to 80% of diagnostic errors in emergency medicine, exposing a critical gap in current clinical practice [1-2]. These oversights often occur due to subtle symptoms or the technical limitations of conventional imaging modalities.

The standard diagnostic methods include X-ray radiography, computed tomography (CT), magnetic resonance imaging (MRI), and ultrasound (US). While effective, each has drawbacks. X-rays can fail to

Prince O. Siaw, Ebenezer Adjei, Ahmad Aldelemy, Aslan N. Moqadam, Mohammed Lashab and Raed A. Abd-Alhameed, "SRR-Based RF Sensor for Non-Invasive Detection of Static Bone Fracture States", *Annals of Emerging Technologies in Computing (AETiC)*, Print ISSN: 2516-0281, Online ISSN: 2516-029X, pp. 32-42, Vol. 9, No. 5, 25 October 2025, Published by International Association for Educators and Researchers (IAER), DOI: 10.33166/AETiC.2025.05.003, Available: http://aetic.theiaer.org/archive/v9/v9n5/p3.html.

detect hairline or occult fractures, especially in anatomically complex regions [3-4]. CT and MRI offer superior resolution but are expensive, time-consuming, and expose patients to ionising radiation (in the case of CT). Ultrasound is radiation-free but is highly operator-dependent and offers limited penetration through bone.

This study introduces a metamaterial-inspired RF sensor that utilises a dual Split-Ring Resonator (SRR) architecture to enhance fracture detection in bone tissue. Operating in the microwave S-band (1–3 GHz), the sensor is designed to detect high-sensitivity dielectric contrasts at fracture sites. This work builds upon preliminary findings presented in [5] and extends prior research by designing a sensor specifically for sub-millimetre defect detection, employing anatomically layered phantoms for enhanced realism, and demonstrating clear resonance shifts as a function of the fracture's state.

2. Related Work and Comparative Analysis

The exploration of non-ionising modalities for medical diagnostics has gained significant traction, with a rich field of research into microwave sensors for various biomedical applications [6-7]. These methods leverage the distinct dielectric properties—permittivity (ϵr) and conductivity (σ)—of biological tissues, which have been extensively modelled by foundational studies [8-9]. A bone fracture introduces a localised dielectric anomaly (e.g., an air gap or blood-filled haematoma) that can be detected by microwave systems [10].

Microwave imaging (MWI) has been investigated for bone fractures, but early work by Santos *et al.* [11] struggled to achieve the resolution needed for micro-fractures. Other approaches have used alternative hardware, such as the compact monopole antenna proposed [12], or to improve diagnostic accuracy, some studies have incorporated machine learning [13].

developed a microwave sensor paired with a deep neural network. Their system could detect cracks between 1-3 mm but relied on simplified cylindrical bone geometries. This simplification, while effective for algorithmic training, limits the direct clinical applicability of the findings, as real anatomical structures are far more complex and heterogeneous. This points to another research gap: the need for validation using more anatomically realistic models.

To overcome these resolution challenges, recent research has focused on metamaterials, particularly Split-Ring Resonators (SRRs), which offer exceptional electromagnetic field confinement [14-16]. The high sensitivity of SRRs has been successfully demonstrated in other fields, such as for characterising fluids in microfluidic channels [17], a principle that directly applies to detecting blood within a fracture site. The table below provides a comparative analysis of these approaches. Another study in [18] utilised an SRR array with a microwave transceiver, achieving high-resolution imaging of narrow fractures (sub-millimetre to 2 mm) at 2.45 GHz. Their work underscored the potential of SRRs but focused on advanced imaging systems with complex arrays.

2.1. Justification for the Present Work

The literature reveals a clear need for a sensor that is non-ionising, low-cost, and capable of detecting sub-millimetre fractures within an anatomically realistic context. While previous studies have made significant progress, they have been limited by either low resolution [11], oversimplified models [13], or complex system architectures [18]. This study aims to fill this gap by proposing a compact, dual-SRR sensor specifically optimised for high sensitivity to sub-millimetre defects. By validating the design on a realistic, multi-layer femur phantom, this work directly addresses the limitations of previous models and demonstrates a clear path toward a clinically viable diagnostic tool. The comparative analysis is summarised in Table 1.

2.2. Comparative Analysis of Related Work

A comparative summary of relevant studies in microwave-based bone fracture detection, contrasting their methodologies and findings with the present work. This analysis highlights the novelty of our proposed sensor, particularly in its ability to detect sub-millimetre fractures using an anatomically realistic phantom. As shown in table (1) below:

Table 1. Comparative Analysis of Related Work

[Ref]	Sensor Type	Freq	Phantom Model	Detected Fracture Size	Key Limitation or Focus
[11]	Microwave Imaging System	1-4 GHz	Three-layer cylindrical model (skin, fat, bone).	Macro-fractures only	Lacked resolution for detecting micro-fractures.
[13]	Microwave Sensor with Deep Neural Network	1-8 GHz	Simplified bone geometries	Cracks of 1-3 mm width	Relied on simplified models, limiting clinical applicability.
[18]	Microwave Transceiver with SRR Array	2.45 GHz	Three-layer phantom simulating human arm tissue	Narrow bone fractures (sub-millimetre to 2 mm)	Focused on high-resolution imaging using advanced antenna arrays.
This Work	**Dual Split-Ring Resonator (SRR) RF Sensor**	**1–3 GHz**	**Anatomically layered femur**	**As small as 0.10 mm**	**Contribution: high sensitivity for sub-millimetre defect detection in a realistic, multi-layer phantom.**

3. Materials and Method

3.1. Anatomically Realistic Femur Phantom and Dielectric Properties

To ensure clinical relevance, a detailed multi-layer phantom of a human femur was developed in CST Microwave Studio. The model replicates the natural shape and tissue composition around the femoral shaft, including layers for skin, fat, muscle, and cortical bone. As microwaves attenuate when passing through these layers, a highly sensitive sensor is essential for accurate detection. The phantom layers and their respective thicknesses are detailed in Table 2, and their frequency-dependent dielectric properties are listed in Table 3. In a fracture event, blood accumulation alters the local dielectric environment, which is a key component of the detection mechanism.

Table 2. Geometric and Dielectric Properties of the Multi-Layer Femur Phantom at 2.5 GHz

Tissue Layer	Thickness (mm)	Relative Permittivity (εr)	Electrical Conductivity (σ, S/m)
Skin	2	37.5	1.74
Subcutaneous Fat	7.5	10.7	0.34
Muscle (Quadriceps)	35	52.1	2.15
Cortical Bone	20	11.1	0.51
Blood (in fracture)	N/A	57.4	3.08

Table 3: Dielectric Properties of Human Tissues at 2.0, 2.5, and 3.0 GHz

Tissue	**Freq. (GHz)**	**Relative Permittivity (ε_r)**	**Electrical Conductivity (σ, S/m)**
Blood	2.0	58.2	2.91
2.5	57.4	3.08	
3.0	56.6	3.25	
Bone (Cortical)	2.0	11.4	0.49
2.5	11.1	0.51	
3.0	10.8	0.53	
Fat	2.0	11.0	0.33
2.5	10.7	0.34	
3.0	10.4	0.35	
Muscle	2.0	53.0	2.05
2.5	52.1	2.15	
3.0	51.3	2.25	
Skin	2.0	38.4	1.65
2.5	37.5	1.74	
3.0	36.6	1.83	

The femur phantom consists of various tissues, including skin, muscle, bone, blood, and fat. The muscle layer attenuates microwave penetration, reducing detection accuracy; thus, a highly sensitive sensor is essential.

A cylindrical model of the femur was initially developed and later refined to replicate natural femur shape and tissue composition, as shown in fig. (1-3). The phantom includes various tissues, including skin, fat, muscle, bone (cortical), and blood. The femoral shaft is composed of osseous structures, with the medial portion positioned beneath the skin and covered by the surrounding tissues. These tissue layers attenuate microwave penetration, reducing the accuracy of fracture detection. Consequently, a highly

sensitive sensor is essential for reliable monitoring. In the event of a fracture, ruptured blood vessels result in blood accumulation, affecting the dielectric properties of the surrounding tissues.

While biological factors such as age, gender, and diet can influence tissue dielectric properties, these variations were not explicitly modelled in this study. Future work may explore the impact of these factors.

3.2. Full-Wave Simulation Setup

All simulations were performed using the Time Domain Solver in CST Microwave Studio® 2024 with adaptive mesh refinement to ensure numerical accuracy. The sensor was placed in direct contact with the skin layer of the femur phantom, as shown in Figures 1-2. The system's response was evaluated by analysing the reflection coefficient (|S11|) at the sensor's input port over a frequency range of 2.0 to 3.0 GHz. Four primary scenarios were simulated to assess the sensor's diagnostic capabilities:

1. Healthy Bone: The intact bone phantom, establishing the baseline resonant frequency.
2. Fractured Bone: A 0.10 mm wide transverse gap was introduced into the cortical bone layer, filled with material properties corresponding to blood.
3. Healed Bone: The fracture gap was filled with a material model representing denser, calcified tissue to simulate a healed state.
4. Blood Extended into Tissue: A scenario modelling a more severe injury where the haematoma extends beyond the bone into surrounding tissue.

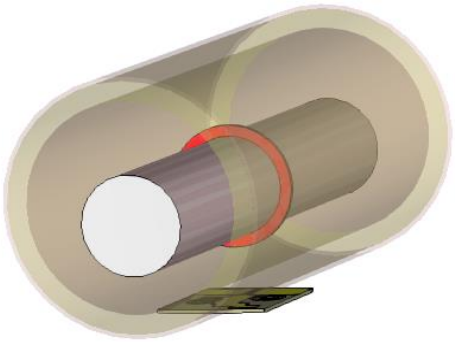

Figure 1. Lateral view of the phantom showing the side view of the bone with a fracture.

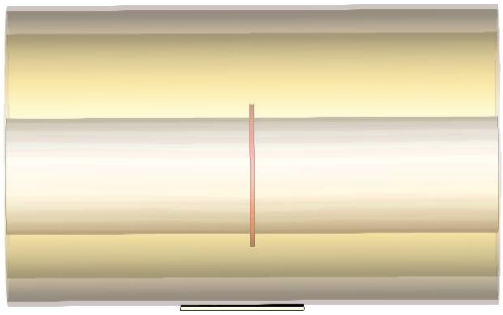

Figure 2. Side view of the position of a monostatic sensor.

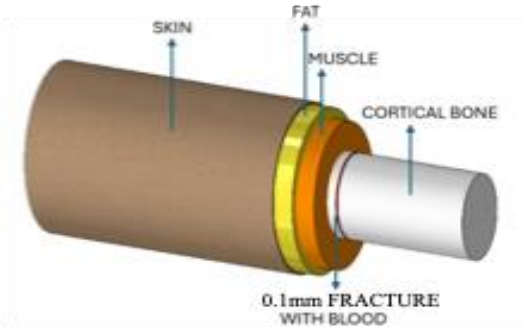

Figure 3. Slightly tilted front view of the bone phantom with tissue layers

3.3. Sensor Design & Theoretical Principle

The proposed sensor is based on a dual Split-Ring Resonator (SRR) architecture, designed to operate between 1.0–3.0 GHz. SRRs function as LC resonant circuits, where the ring acts as an inductor and the gap between the rings acts as a capacitor. The resonant frequency (fr) can be approximated by:

$$f_r \approx \frac{1}{2\pi\sqrt{L_{eff}C_{eff}}} \quad (1)$$

Here, L_{eff} represents the effective inductance of the ring structure, and C_{eff} represents the effective capacitance, which is primarily influenced by the gap in the ring and the dielectric material nearby.

The sensing principle relies on near-field perturbation. The SRR's split-gap structure creates a highly confined and intense electric field. When the sensor is placed on tissue, the tissue's dielectric properties become part of the sensor's effective capacitance (C_{eff}). Any change in the tissue's relative permittivity (ϵr), such as a fracture filled with blood, causes a shift in this capacitance, leading to a measurable shift in the resonant frequency (Δfr). The sensor was implemented on a 0.80 mm thick FR-4 substrate (ϵr = 4.3, $\tan\delta$ = 0.025) with compact dimensions of 30.00 mm × 25.00 mm.

3.4. Iterative Sensor Design and Optimisation (ANT 1 to ANT 5)

The final sensor configuration was achieved through a systematic, iterative design process aimed at maximising sensitivity and ensuring robust performance when loaded with the tissue phantom. This evolution, from ANT 1 to the optimised ANT 5, is depicted in Figure 4, with the corresponding simulated reflection coefficients shown in Figure 5.

- ANT 1 (Baseline Design): The process began with a basic single-ring SRR coupled to a microstrip feedline. Simulations showed a resonant response, but the resonance was broad (low Q-factor) and shallow, indicating poor field confinement and inefficient energy coupling.
- ANT 2 & 3 (Geometric Tuning): Successive modifications involved systematically varying the geometric parameters of the single ring, including its radius, conductor width, and gap width. These stages yielded incremental improvements in the Q-factor but failed to achieve the sharp, deep resonance required for high-resolution sensing.
- ANT 4 (Dual-SRR Introduction): A significant architectural change was made by introducing a second, coupled SRR. This dual-resonator configuration leverages electromagnetic coupling to enhance the resonant behaviour, resulting in a much sharper and deeper resonance notch in the reflection coefficient, which corresponds to a higher Q-factor and stronger field confinement.
- ANT 5 (Final Optimisation): The final design, ANT 5, involved fine-tuning the dual-SRR geometry. Specific adjustments, including notch modifications in the feedline and alterations to the ring symmetry, were implemented. These final refinements were specifically aimed at optimising the impedance matching between the sensor and the multi-layer tissue phantom. This optimisation is evidenced by the exceptionally deep reflection coefficient minimum (S11) achieved in the final loaded simulations.

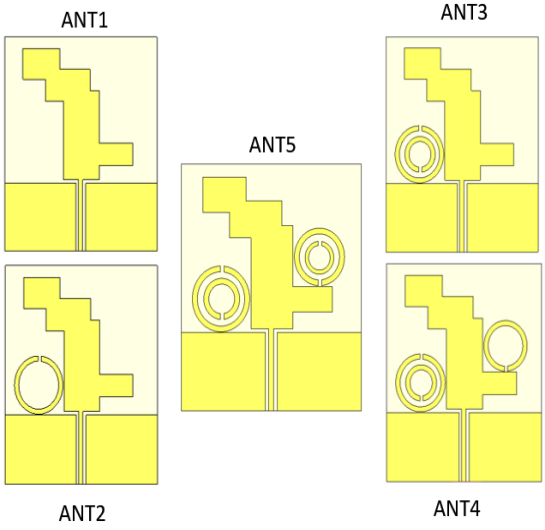

Figure 41. Design stages of the proposed antenna

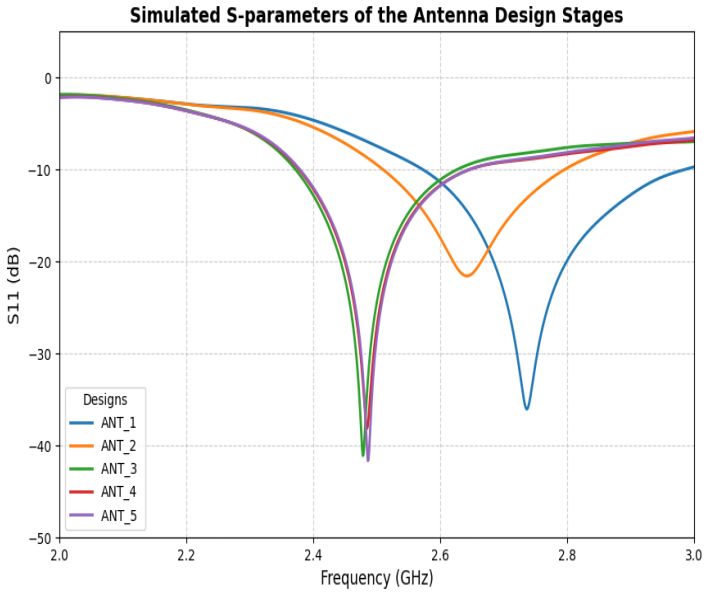

Figure 52. Simulated S-parameters of all ANT design stages

4. Results and Analysis

The performance of the optimised sensor (ANT 5) was rigorously evaluated by simulating its response to the different bone conditions. The results demonstrate clear, distinguishable responses for each state, providing strong evidence for the sensor's diagnostic potential.

4.1. Resonant Response to Fractured States

Figure 6a presents the simulated reflection coefficient (|S11|) of the sensor when loaded with the phantom under various conditions. When placed on the healthy bone phantom, the sensor established a baseline resonance at 2.470 GHz. In the primary fracture scenario ("Blood Within Bone"), the resonant frequency shifted down significantly by 47 MHz to 2.423 GHz. For the healed fracture state, the frequency was 2.452 GHz, a smaller but still distinct downward shift of 18 MHz relative to the healthy baseline. The unique and clearly separable frequency signature for each state is evident in the zoomed-in view (Figure 6b), Similarly with a simulated reflection coefficient (S11) of the sensor in free space, without tissue loading

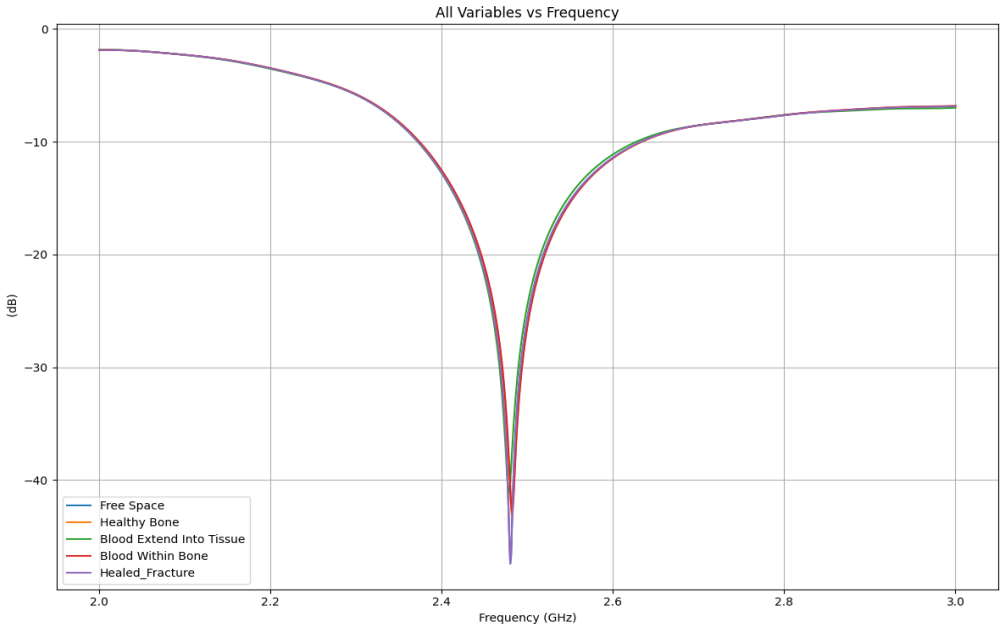

(a)

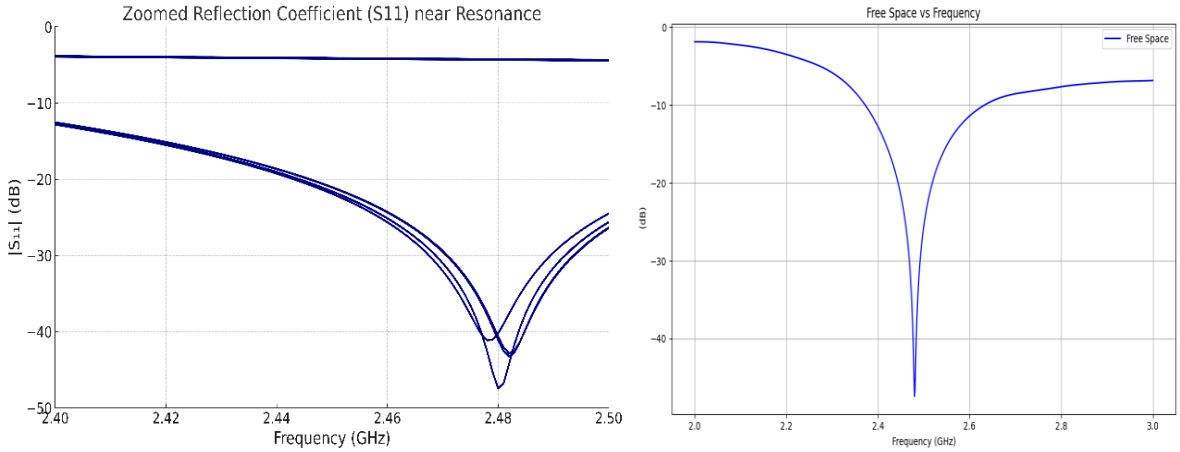

(b) (c)

Figure 6. (a) Simulated reflection coefficient (S11) of the proposed SRR-based sensor in contact with the bone phantom under different fracture conditions, showing resonant frequency shifts; (b) A zoomed-in plot around the resonance shifts region (2.4-2.5 GHz) and (6c) the simulated reflection coefficient (S11) of the sensor in free space, without tissue loading

4.2. Analysis of Diagnostic Sensitivity and Resolution

The large 47 MHz frequency shift observed for the fractured state is the primary diagnostic indicator. This shift is a direct consequence of the physics of resonant perturbation outlined in Section 3.2. The fracture gap, when filled with blood, introduces a region of very high relative permittivity ($\epsilon_r \approx 57.4$) directly into the sensor's most sensitive near-field region. This is in stark contrast to the low permittivity of the surrounding cortical bone ($\epsilon_r \approx 11.1$). This high-contrast dielectric anomaly dramatically increases the local effective capacitance (C_{eff}) of the SRR, causing the pronounced downward shift in resonant frequency.

The high sensitivity derived from this mechanism enables the detection of fractures as small as 0.10 mm in width, even when located 20 mm deep within the cortical bone layer. This represents a significant advancement in resolution compared to prior art. For context, previous microwave imaging systems were often limited to detecting only macro-fractures, and other sensor designs combined with neural networks could resolve cracks only in the 1–3 mm range. The ability to detect sub-millimetre features demonstrates a key strength of the proposed dual-SRR design, addressing a critical limitation of previous work. Furthermore, the ability to distinguish between healthy, fractured, and healed states suggests the sensor's potential for not just initial diagnosis but also for non-invasively tracking patient recovery, a concept supported by studies showing changes in bone's electrical properties during the healing process.

4.3. Signal Integrity and Potential for Clinical Reliability

Beyond the magnitude of the frequency shifts, the quality of the resonance signal itself underscores the sensor's robust design and potential for clinical reliability. As shown in Table 3, the reflection coefficient (|S11|) for the healthy bone state reached a minimum of –47.0 dB. This extremely low value indicates that nearly all the input energy was efficiently coupled into the sensor-tissue system at resonance, signifying excellent impedance matching. Such strong coupling is vital for maximising the signal-to-noise ratio in a practical application, ensuring that the diagnostic signal is strong and clear.

Moreover, the sensor maintained a high-quality factor (Q-factor), ranging from 77.4 to 82.1 across all tested conditions. The Q-factor is a measure of the sharpness of the resonance peak. A high Q-factor, as achieved here, is critically important for clinical reliability for two reasons. First, it ensures that the resonance is a sharp, narrow dip rather than a broad, shallow one, making the precise resonant frequency easy and unambiguous to determine. Second, it allows for the clear separation of closely spaced frequencies. As seen in Figure 5b, the distinct peaks for healthy, healed, and fractured states are clearly distinguishable, which minimises the risk of misdiagnosis. This high performance in both impedance

matching and Q-factor is a direct result of the iterative design process that optimised the dual-SRR geometry for high field confinement and sensitivity.

Table 4. Summary of Simulated Sensor Response under Varying Bone Conditions

Condition	Resonant Frequency (GHz)	|S11| (dB)	Δf (MHz)	Q-Factor
Healthy Bone	2.470	–47.0	–	82.1
Blood Extended into Tissue	2.440	–41.3	30	79.2
Blood Within Bone	2.423	–38.5	47	77.4
Healed Fracture	2.452	–43.8	18	80.7

The quality factor (Q) was calculated using the following formula:

$$Q = \frac{f_r}{FWHM} \quad (2)$$

where f_r is the resonant frequency and FWHM represents the full width at half maximum of the |S11| response.

4.4. Electromagnetic Field Confinement and Sensing Mechanism

To visually demonstrate the sensing mechanism, the simulated surface current and electric field distributions at the resonant frequency are shown in Figure 7 and the sensor's geometry in Figure 8. The underlying physics of the sensor's high sensitivity is rooted in its ability to generate and confine intense electromagnetic fields in a very small, sub-wavelength volume [21].

The surface current plot (Figure 7) confirms the strong resonant behaviour in the dual-ring structure. At the resonant frequency, the incident microwave energy efficiently excites strong, circulating currents within the metallic rings. This resonant current flow is fundamental to establishing the strong magnetic and electric fields that define the sensor's operation [22].

The gaps in the SRRs function as capacitors, where charge accumulates on opposite sides, creating a powerful and highly localised electric field. This region of maximum field intensity is the "sensing hot-spot". It is this concentration of energy that makes the sensor exceptionally sensitive to dielectric changes occurring directly beneath it in the near field. The interaction between this confined field and the material under test is the core of the sensing principle. When the high-permittivity blood from a fracture enters this hot-spot, it dramatically increases the effective capacitance of the gaps, which in turn causes the large, measurable downward shift in the sensor's resonant frequency, visually confirming the source of the sensor's high sensitivity [23].

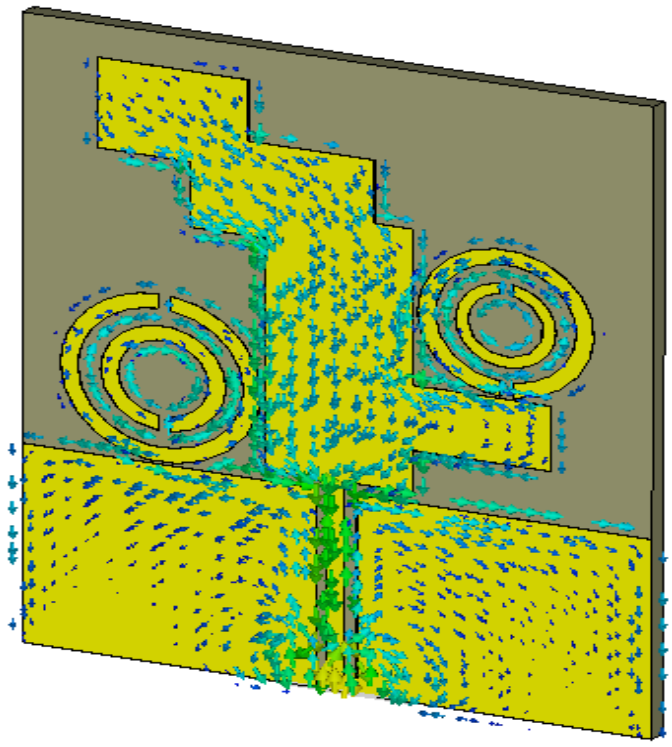

Figure 7. Surface current of the proposed sensor at (f=2GHz)

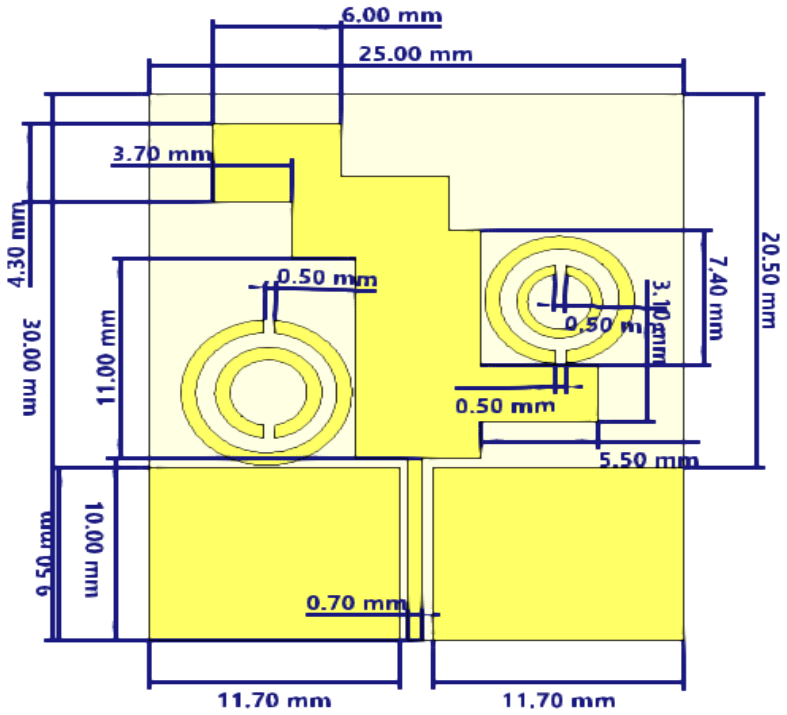

Figure 8. Proposed sensor with its dimensions

Table 5. Dimensions of the proposed microwave sensor

Parameter	Dimension (mm)	Parameter	Dimension (mm)
Feedline length	10	Bottom left vertical height	11
Feedline width	0.7	Horizontal offset (top step)	6
Lower patch left width	11.7	Top left notch offset	25
Lower patch right height	9.5	Ring 1: Left inner radius	1.5
Top right inset height	3.1	Ring 1: Outer radius	2
Middle right section height	7.4	Ring 2: Right inner radius	3.3
Middle left section height	4.3	Ring 2: Outer radius	4

5. Conclusion and Future Work

This study successfully demonstrated, through full-wave simulations, the potential of a metamaterial-based dual-SRR sensor for the non-invasive detection of static bone fracture states. Validated on an anatomically realistic femur phantom, the sensor exhibited high sensitivity to fracture-induced dielectric variations, capable of detecting features as small as 0.10 mm. The distinct and measurable frequency shifts between healthy, fractured, and healed bone conditions, combined with the high signal quality (high Q-factor and excellent impedance matching), underscore the sensor's diagnostic promise.

It is important to acknowledge the limitations of this study. The results are currently based on simulations of idealised, static scenarios. The current model only investigates a single type of transverse fracture, and the potential impact of inter-patient variability in tissue dielectric properties was not explored.

Future work will advance this research toward clinical application along four key avenues. First, the immediate next step is to fabricate a prototype of the optimised sensor and validate its performance using physical, tissue-mimicking phantoms, cross-validating the results against established measurement techniques. Second, we will explore the fabrication of the sensor on a flexible substrate, such as polyimide or PDMS, to create a conformal, wearable prototype suitable for long-term monitoring. Low-cost manufacturing techniques like screen printing or inkjet printing are viable options for producing such flexible electronic sensors. Third, pending ethical approval, *in vivo* studies will be planned to track the healing process over time, correlating sensor readings with medically relevant metrics of bone repair. Finally, we will investigate the integration of the sensor with machine learning algorithms to automate the classification of bone states, which could enhance diagnostic accuracy and create a "smart" system for real-time orthopaedic assessment.

CRediT Author Contribution Statement

Prince O. Siaw: Conceptualisation, Methodology, Software, Validation, Writing – Original Draft. Ebenezer Adjei: Software, Validation. Ahmad Aldelemy: Visualisation, Investigation. Aslan N. Moqadam: Methodology, Writing – Review & Editing. Mohammed Lashab: Formal analysis. Raed A. Abd-Alhameed: Conceptualisation, Supervision, Project Administration, Funding Acquisition, Writing – Review & Editing.

Acknowledgement

This work is partially supported by the UK Engineering and Physical Sciences Research Council (EPSRC) under grant EP/X039366/1, and HORIZON-MSCA-RISE ID: 101086492, Marie Skłodowska-Curie, Research and Innovation Staff Exchange (RISE), titled: FractuRe Orthopaedic Rehabilitation: Ubiquitous eHealth Solution (Robust).

References

[1] Anita Deakin, Timothy J. Schultz, Kim Hansen and Carmel Crock, "Diagnostic error: Missed fractures in emergency medicine", in *Emergency Medicine Australasia*, ISSN: 1742-6731, Vol. 27, No. 2, pp. 177-178, 19 November 2014, Published by Wiley, DOI: 10.1111/1742-6723.12328, Available: https://onlinelibrary.wiley.com/doi/10.1111/1742-6723.12328.

[2] Xiaoxuan Liu, Livia Faes, Aditya U. Kale, Siegfried K. Wagner, Dun Jack Fu *et al.*, "A comparison of deep learning performance against health-care professionals in detecting diseases from medical imaging: a systematic review and meta-analysis", in *The Lancet Digital Health*, ISSN: 2589-7500, Vol. 1, No. 6, pp. e271-e297, 9 October 2019, Published by Elsevier, DOI: 10.1016/s2589-7500(19)30123-2, Available: https://www.thelancet.com/journals/landig/article/PIIS2589-7500(19)30123-2.

[3] Farida Wahyuni, Setyawan P. Sakti, Dionysius J. D. H. Santjojo, Unggul P. Juswono and Didik. R. Santoso, "The effect of delay time processing on exposure index in x-ray examination", in *Proceedings of the International Conference on Science And Applied Science (ICSAS2020)*, 7 July 2020, Surakarta, Indonesia, ISBN: 978-0-7354-4068-0, Published by AIP Publishing, DOI: 10.1063/5.0030629, Available: https://pubs.aip.org/aip/acp/article/2296/1/020117/724219.

[4] Siyuan Yang, Boran Yin, Wei Cao, Chao Feng, Guodong Fan *et al.*, "Diagnostic accuracy of deep learning in orthopaedic fractures: a systematic review and meta-analysis", in *Clinical Radiology*, ISSN: 0009-9260, Vol. 75, No. 9, pp. 713.e17-713.e28, 23 June 2023, Published by Elsevier, DOI: 10.1016/j.crad.2020.05.021, Available: https://pubmed.ncbi.nlm.nih.gov/32591230/ .

[5] Prince O. Siaw, Mohammed Lashab, Ebenezer Adjei, Ahmad Aldelemy, Ahmed S. I. Amar *et al.*, "Optmized Metamaterial Sensor for Effective Bone Fracture Detection", in *Proceedings of the 2024 International Telecommunications Conference (ITC '24)*, 22-25 July 2024, Cairo, Egypt, ISBN: 979-8-3503-7505-8, pp. 657-660, Published by IEEE, DOI: 10.1109/itc-egypt61547.2024.10620473, Available: https://ieeexplore.ieee.org/document/10620473.

[6] Cristina Origlia, David O. Rodriguez-Duarte, Jorge. A. Tobon Vasquez, Jean-Charles Bolomey and Francesca Vipiana, "Review of Microwave Near-Field Sensing and Imaging Devices in Medical Applications", in *Sensors*, ISSN: 1424-8220, Vol. 24, No. 14, p. 4515, 12 July 2024, Published by MDPI, DOI: 10.3390/s24144515, Available: https://www.mdpi.com/1424-8220/24/14/4515.

[7] Isah Musa Danjuma, Salamatu Abubakar Ibrahim, Prince Siaw, Ahmed S. I. Amar, Shaza M. EL-Nahass *et al.*, "Rectangular Slotted Monopole Antenna Design for Breast Cancer Tumor Detection", in *Proceedings of the 2024 International Telecommunications Conference (ITC '24)*, 22-25 July 2024, Cairo, Egypt, ISBN: 979-8-3503-5140-8, pp. 672-676, Published by IEEE, DOI: 10.1109/itc-egypt61547.2024.10620468, Available: https://ieeexplore.ieee.org/document/10620468.

[8] William T. Joines, Yang Zhang, Chenxing Li and Randy L. Jirtle, "The measured electrical properties of normal and malignant human tissues from 50 to 900 MHz", in *Medical Physics*, ISSN: 0094-2405, Vol. 21, No. 4, pp. 547-550, April 1994, Published by Wiley, DOI: 10.1118/1.597312, Available: https://aapm.onlinelibrary.wiley.com/doi/10.1118/1.597312.

[9] Sami Gabriel, Rita W. Lau and Camelia Gabriel, "The dielectric properties of biological tissues: III. Parametric models for the dielectric spectrum of tissues", in *Physics in Medicine and Biology*, ISSN: 0031-9155, Vol. 41, No. 11, pp. 2271-2293, November 1996, Published by IOP Publishing, DOI: 10.1088/0031-9155/41/11/003, Available: https://iopscience.iop.org/article/10.1088/0031-9155/41/11/003.

[10] Ahmad Aldelemy, Ebenezer Adjei, Prince Siaw, John Buckley, Maryann Hardy *et al.*, "'Exploring Radio Frequency Techniques for Bone Fracture Detection: A Comprehensive Review of Low Frequency and Microwave Approaches'", in *Annals of Review and Research*, ISSN: 2578-8883, Vol. 10, No. 1, 13 September 2023, Published by Juniper Publishers, DOI: 10.19080/arr.2023.10.555778, Available: https://juniperpublishers.com/arr/ARR.MS.ID.555778.php.

[11] Kesia C. Santos, Carlos A. Fernandes and Jorge R. Costa, "Feasibility of Bone Fracture Detection Using Microwave Imaging", in *IEEE Open Journal of Antennas and Propagation*, ISSN: 2637-6431, Vol. 3, pp. 836-847, 27 July 2022, Published by IEEE, DOI: 10.1109/OJAP.2022.3194217, Available: https://ieeexplore.ieee.org/document/9843919.

[12] Ananda V. Boologam, Kalimuthu Krishnan, Sandeep K. Palaniswamy, Sachin Kumar, Shreya Bhaowmik *et al.* "On the Design and Development of Planar Monopole Antenna for Bone Crack/Void Detection", in *International Journal of Antennas and Propagation*, ISSN: 1687-5869, Vol. 2022, p. e4663488, 5 May 2022, Published by Hindawi, DOI: 10.1155/2022/4663488, Available: https://onlinelibrary.wiley.com/doi/10.1155/2022/4663488.

[13] Sina Beyraghi, Fardin Ghorbani, Javad Shabanpour, Mir E. Lajevardi, Vahid Nayyeri *et al.*, "Microwave bone fracture diagnosis using deep neural network", in *Scientific Reports*, ISSN: 2045-2322, Vol. 13, No. 1, p. 16957, 7 October 2023, Published by Nature, DOI: 10.1038/s41598-023-44131-5, Available: https://www.nature.com/articles/s41598-023-44131-5.

[14] John B. Pendry, Aidan J. Holden, David J. Robbins and William J. Stewart, "Magnetism from conductors and enhanced nonlinear phenomena", in *IEEE Transactions on Microwave Theory and Techniques*, Print ISSN: 0018-9480, Online ISSN: 1557-9670, Vol. 47, No. 11, pp. 2075-2084, 30 November 1999, Published by IEEE, DOI: 10.1109/22.798002, Available: https://ieeexplore.ieee.org/document/798002.

[15] Hou-Tong Chen, Willie J. Padilla, Joshua M. O. Zide, Arthur C. Gossard, Antoinette J. Taylor *et al.*, "Active terahertz metamaterial devices", in *Nature*, ISSN: 1476-4687, Vol. 444, No. 7119, pp. 597-600, 1 November 2006, Published by Nature, DOI: 10.1038/nature05343, Available: https://www.nature.com/articles/nature05343.

[16] David R. Smith, John. B. Pendry and Michael. C. K. Wiltshire "Metamaterials and Negative Refractive Index", in *Science*, ISSN: 1095-9203, Vol. 305, No. 5685, pp. 788-792, 6 August 2004, Published by AAAS, DOI: 10.1126/science.1096796, Available: https://www.science.org/doi/10.1126/science.1096796.

[17] Arash Ebrahimi, Withawat Withayachumnankul, Said Al-Sarawi and Derek Abbott, "High-Sensitivity Metamaterial-Inspired Sensor for Microfluidic Dielectric Characterization", in *IEEE Sensors Journal*, Print ISSN: 1558-1748, Online ISSN: 1530-437X Vol. 14, No. 5, pp. 1345-1351, 18 December 2013, Published by IEEE, DOI: 10.1109/jsen.2013.2295312, Available: https://ieeexplore.ieee.org/document/6687229.

[18] Aslan Nouri Moqadam and Reza Kazemi, "High-Resolution Imaging of Narrow Bone Fractures With a Novel Microwave Transceiver Sensor Utilizing Dual-Polarized RIS and SRR Array Antennas", in *IEEE Sensors Journal*, Print ISSN:1558-1748, Online ISSN: 1530-437X vol. 23, no. 24, pp. 30335-30344, 02 November 2023, Published by IEEE, DOI: 10.1109/jsen.2023.3328240, Available: https://ieeexplore.ieee.org/document/10305514.

[19] Siyu Li, Shaowei Liao, Yang Yang, Wenquan Che and Quan Xue, "Low-Profile Circularly Polarized Isoflux Beam Antenna Array Based on Annular Aperture Elements for CubeSat Earth Coverage Applications", in *IEEE Transactions on Antennas and Propagation*, Print ISSN: 0018-926X, Online ISSN**:** 1558-2221, Vol. 69, No. 9, pp. 5489-5502, 24 February 2021, Published by IEEE, DOI: 10.1109/tap.2021.3060039, Available: https://ieeexplore.ieee.org/document/9362214.

[20] Marjolein C. H. van der Meulen, Xu Yang, Timothy G. Morgan and Mathias P. G. Bostrom, "The Effects of Loading on Cancellous Bone in the Rabbit", in *Clinical Orthopaedics & Related Research*, ISSN: 1528-1132, Vol. 467, No. 8, pp. 2000-2006, 21 May 2009, Published by Springer, DOI: 10.1007/s11999-009-0897-4, Available: https://link.springer.com/article/10.1007/s11999-009-0897-4.

[21] Irfan Bulu, Humeyra Caglayan, Koray Aydin and Ekmel Ozbay, "Compact size highly directive antennas based on the SRR metamaterial medium", in *New Journal of Physics*, ISSN: 1367-2630, Vol. 7, No. 1, p. 223, 20 October 2005, Published by IOP Publishing, DOI: 10.1088/1367-2630/7/1/223, Available: https://iopscience.iop.org/article/10.1088/1367-2630/7/1/223.

[22] Fabian Vazquez, Alejandro Villareal, Alfredo Rodriguez, Rodrigo Martin, Sergio Solis-Najera *et al.*, "Electric Field Sensing with a Modified SRR for Wireless Telecommunications Dosimetry", in *Electronics*, ISSN: 2079-9292, Vol. 10, No. 3, p. 295, 26 January 2021, Published by MDPI, DOI: 10.3390/electronics10030295, Available: https://www.mdpi.com/2079-9292/10/3/295.

[23] Ali M. Albishi, "A Novel Coupling Mechanism for CSRRs as Near-Field Dielectric Sensors", in *Sensors*, ISSN: 1424-8220, Vol. 22, No. 9, p. 3313, 26 April 2022, Published by MDPI, DOI: 10.3390/s22093313, Available: https://www.mdpi.com/1424-8220/22/9/3313.